International Journal of Biological Macromolecules 321 (2025) 145931

Contents lists available at ScienceDirect

International Journal of Biological Macromolecules

journal homepage: www.elsevier.com/locate/ijbiomac

Hybrid biocomposites: From molecular behaviour to material properties in silk fibroin/cellulose films

James A. King [a], Peter J. Hine [a], Daniel L. Baker [a], Matthew Creswick [b], Michael E. Ries [a,*]

[a] School of Physics and Astronomy, University of Leeds, Leeds, LS2 9JT, West Yorkshire, UK
[b] School of Chemical and Process Engineering, University of Leeds, Leeds, LS2 9JT, West Yorkshire, UK

ARTICLE INFO

Keywords:
Silk fibroin
Cellulose
Ionic liquid
Biomaterial
Mechanical testing

ABSTRACT

Hybrid biomaterials of silk fibroin and cellulose offer improvements over single-component alternatives in the pursuit of optimised and sustainable materials: showing superior strength, biocompatibility, and flexibility. We investigate the behaviours of fully dissolved and coagulated hybrid films at various compositions and characterise the system with X-ray diffraction, dynamic mechanical thermal, thermogravimetric, and mechanical analyses. We confirm a system optimum in modulus, maximum strength, and maximum strain at failure (2.2 GPa, 28 MPa, and 3.3% respectively) at 85%–95% cellulose and 5%–15% silk fibroin hybrid composition. Thermogravimetric analysis indicates this is due to increasing interaction density in hybrid compositions correlated with the formation of a hybrid mixed phase up to 4 wt%. We recreate conflicting trends in literature showing sample flexibility improving and reducing with addition of silk fibroin and indicate this is due to variations in sample creep and strain rate. We report a slow stress relaxation and time-dependent viscoelasticity causing this, using comparative mechanical tests at different rates of deformation. We propose a slipping mechanism for stress relaxation similar to those seen in other biopolymer-based biological systems, for example actin filaments in cytoskeletons.

1. Introduction

The negative impact of petrochemical plastic use on the climate necessitates sustainable alternatives to conventional plastics, such as biologically derived materials [1–4]. These can take the form of natural-fibre reinforced materials, self supporting biopolymer composites or bioplastics formed of biopolymer networks [5–7]. Taking advantage of the high performance and sustainability of these may offer beneficial results with applications in the biomedical, structural, or aerospace fields [8–11]. Two abundant structural biopolymers key to these developments are cellulose and silk fibroin (SF).

Silk is a fibrous protein extrusion hierarchically structured of silk sericin and SF proteins. SF provides structural strength and, though the chemical composition varies, typically has a hexapeptide primary sequence of mostly glycine amino acid units as shown in Fig. 1(a) [12]. Cellulose is an anisotropic, abundant, biocompatible polymer. It is formed of repeat units of anhydroglucose monomers in the lowest energy ring conformation: D-glucopyranose [8,13]. β-1,4-glycosidic bonds between these units then form dissacharide units of anhydrocellobiose, which can be seen in Fig. 1 (b) [14]. This unique structure gives rise to Young's moduli of up to 200 GPa, and an ultimate tensile strength of up to 17.8 GPa [15]. This is 7 times stronger than typical steel with a fifth of steel's density [15].

Combining SF and cellulose into hybrid biomaterials offers unique compatibility and useful properties that surpasses other composite examples [16–20]. Inclusion of SF can improve the biocompatibility of the cellulose bioplastic and aid in biomedical applications [21]. Hybrid materials have also shown improved strain at failure and maximum stress compared to pure cellulose or SF counterparts [22,23]. This is due to the close molecular associations of SF and cellulose as confirmed by the NMR studies of Tian et al. [22] These show that homogeneous blends of SF and cellulose, as indicated by atomic force microscopy in literature, contain close molecular association between SF and cellulose molecules [18,22,24]. An adaptation of the proposed prominent points of hydrogen bonding are shown in Fig. 2.

Much of the existing literature focuses on applications in biomedical fields [8,12,25], as SF can promote cellular adhesion and proliferation of fibroblasts and keratinocytes [10,26,27]. SF composites can also be biocompatible, biodegradable and non-toxic, though complex biological responses render biocompatability non-universal [16,28]. As biological tissues are individual and unique, biomimetic scaffolds or artificial tissues must be engineered to both replicate extensive tissue properties and regulate healing phases. Artificial tissues must then imitate or trigger the correct immunoresponse signals, which

* Corresponding author.
E-mail addresses: mmjki@leeds.ac.uk (J.A. King), m.e.ries@leeds.ac.uk (M.E. Ries).

https://doi.org/10.1016/j.ijbiomac.2025.145931
Received 3 April 2025; Received in revised form 20 June 2025; Accepted 10 July 2025
Available online 22 July 2025

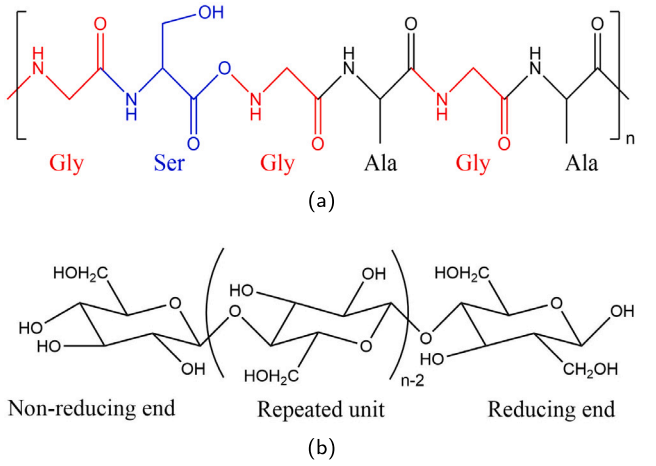

Fig. 1. Example typical molecular sequences for (a) silk fibroin and (b) cellulose repeat units [8]. Amino acid groups are colour coded in the silk fibroin protein.

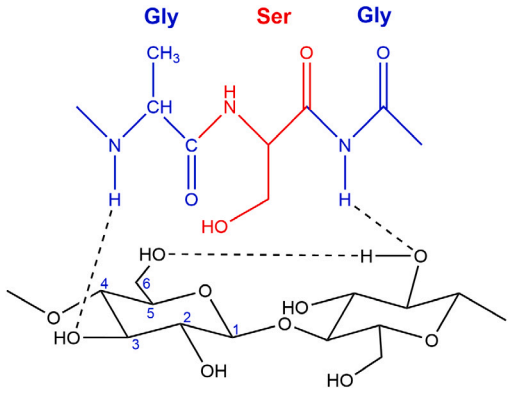

Fig. 2. The proposed molecular interactions of the SF and cellulose chains with example amino acids adapted from work by Tian et al. [22].

has been achieved in hybrid systems [29–33]. These biocomposites can also degrade and resorb *in-vivo*, while conventional alternatives require secondary surgeries [34–37]. Ganguly et al. prepared a hybrid composite scaffold of cellulose nanocrystals with an alginate-SF matrix. This was shown to function effectively *in-vivo* to improve bioactivity and wound healing [38]. Other non-biomedical applications for SF-cellulose hybrid materials exist, including strengthening and restoring tapestries with chemically identical biopolymer solutions [7].

Despite promise shown in the behaviours of hybrid biopolymer composites, the nature of the sample behaviour remains a contentious issue. Many studies indicate a performance increase with a small addition of 5%–30% SF content to a cellulose network [17,22,23,39,40]. Other studies indicate a negative trend in maximum strength or strain at failure with addition of SF [23,41]. Other variations include quoted strains of failure in ranges from 40%–60% by Shang et al. or 8%–10% by Tian et al. [22,39]. These differences are not explained by variations in sample water content between studies, which could induce softening due to disruption of inter- and intramolecular hydrogen bonds [42]. These variations also occur in studies with comparable component sources and preparation techniques. Inconsistencies in reported behaviours may be due to compositional effects and relaxation behaviours not previously considered.

This study investigates relaxation behaviours and molecular/meso-molecular length scale behaviours alongside bulk mechanical measurements to elucidate the contradictory behaviour of these materials beyond previous studies. This could enable improved application beyond already promising investigations into biomedical uses. We prepare fully dissolved and regenerated films of SF and cellulose using ionic liquids as a sustainable solvent with effective dissolution, recyclability, and minimal environmental impact [43–45]. Complete dissolution and homogenous dispersal of polymers avoids retention of undissolved fibres which impacts behaviours based on level of dissolution, level of fibre entanglement, orientation, and fibre-matrix interfaces [5,9,46,47]. This enables us to draw conclusions about fundamental behaviours affecting molecular interactions in all examples of these hybrid materials. We utilise double network theory, and comparisons with relevant biological materials to rationalise contradictions and trends seen within literature. We then establish the presence of a slow stress relaxation and viscoelastic behaviour similar to more complex biological systems [48–50]. Notably, we discuss the variability in strength and flexibility with addition of SF to cellulose materials beyond effects of solvent choice, polymer source, purity, alignment, and level of reinforcement [6,21,23,32]. In this case, films will be studied due to the benefits inherent over more porous samples. These can exhibit reduced bending, tensile, and compressive strength, which must be alleviated by compression [51]. These also show added variation due to porosity, which can affect mechanical properties [51].

2. Experimental section

2.1. Materials

Degummed *Bombyx mori* silk thread was purchased online (mulberry undyed spun silk from Empress Mills, U.K.) and stored under dry conditions. After dissolution this silk is referred to as SF, as it comprises of mostly SF. PH-101 Microcrystalline cellulose was purchased from Avicell with an approximate 50 μm particle size. The ionic liquid, 1-ethyl-3-methylimidazolium acetate (EmimAc), was purchased from Proionic, with a purity of 97%. All EmimAc, cellulose, and silk was dried overnight at 60 °C under vacuum before use. Dimethyl Sulfoxide (DMSO) was purchased from Sigma-Aldrich with a purity of 99.9%. Methanol was purchased from Fisher Scientific, with purity of 98%, for use in washing and coagulation of samples.

2.2. Fabrication

Choices in dissolution and coagulation conditions were made after comparison with literature examples and investigation into efficiencies of different solvent systems as described in our previous studies [8,52,53]. In particular, the solvent ratio was selected based on previous findings probing effective dissolution of SF and cellulose with EmimAc and DMSO solvent mixtures [53].

Cellulose was dissolved at 10 wt% in an 20:80, EmimAc:DMSO mixture of solvents. Silk fibres were dissolved at 10 wt% in a 80:20, EmimAc:DMSO mixture of solvents. Polymeric solids were firstly dispersed in the relevant weight of DMSO, then stirred and preheated to 100 °C for 30 mins. The relevant weight of EmimAc was preheated at 100 °C for 30 mins then mixed with the dispersed solids in DMSO. Solutions were then stirred for 16 h, at 100 °C, at 200 rpm to produce pale yellow to dark amber transparent solutions. SF solutions showed darker colour than cellulose solutions. After dissolution a hybrid solution was prepared by mixing the solution for 30 min, at 100 °C, at 200 rpm. All dissolution was performed in sealed vessels to minimise the effects of humidity. Optical microscopy confirms complete dissolution within our solutions as shown in Figure S1 [53].

Film composition was altered by changing the cellulose:SF weight ratio with the total mass of polymeric solid remaining the same. The polymer solution was poured into a circular petri dish (10 cm diameter) and left to deaerate for 2 h at 70 °C under vacuum. The cast film was then coagulated in a methanol atmosphere statically for 24 h, by placing under a vacuum environment with 200 ml of methanol. The film was then washed in deionised water (5 l) for 48 h. The water was replaced twice in that period. The film was then dried at room

temperature and humidity for 6 h. Films were then pinched between flat metal sheets (≈10 KPa using bulldog clips), to alleviate deformation due to differential shrinkage during drying and cooling, then dried for 24 h at 60 °C. Examples can be seen in Figure S2. Approximately 65%–80% of the original polymeric mass was left after drying the films and higher SF compositions showed higher mass loss during washing. A schematic of the production methodology can be seen in Figure S3.

Before any characterisation, samples were equilibrated under ambient conditions for at least 24 h. The average room humidity was 50 ± 1% and the average temperature was 20.6 ± 0.2 °C. Analysis results were averaged over at least three measurements unless otherwise mentioned. Most analyses in Section 3 discuss properties as a function of SF content with a focus on 0%–50% SF. Qualitatively, it has been found that in fully dissolved blends SF contents over 50% caused mechanically unstable composites [54]. It is widely recorded that pure SF films are brittle and weak [41,55,56].

2.3. Mechanical testing

Tensile tests of the films were carried out on an Instron 5564 universal test machine equipped with a 2 kN calibrated load cell at room temperature. Tests were performed on rectangular strips of 5 mm width and of 30 mm length. Samples were gripped with sandpaper at clamping points to minimise slippage. The gauge length was 25–30 mm. The cross-head speed in the direction parallel to the film was altered as discussed in Section 3.3. The tensile Young's modulus (in the initial linear strain range of 0.0–0.5%) was measured from the resulting stress strain curves.

Quasi-static testing (creep, and stress relaxation tests) was performed in three-point bending fixtures. These were performed on a dynamic mechanical analyser (TA Instruments DMA850.) For creep tests, 8 MPa of stress was applied as this was within the elastic region found from flexural testing for all samples in preliminary flexural tests (see Figure S4.) For stress relaxation tests 1% flexural strain was used as the displacement held, as this was within the elastic region of all samples in flexural testing. The flexural modulus at the maximum stress was calculated from the stress strain curves and was calculated at the outer surface of the test specimen at mid-span. The flexural strain was calculated using the equation for rectangular cross section samples in three-point bending [57]:

$$\epsilon_f = \frac{6Dd}{L^2} \tag{1}$$

where ϵ_f is the strain in the outer surface (mm/mm), D is the maximum displacement of the centre (mm), d is the thickness of the samples (mm), and L is the support span (mm). The flexural stress was calculated using the equation [57]:

$$\sigma_f = \frac{3FL}{2bd^2} \tag{2}$$

where F is the load (N), and b is the width of the sample (mm).

2.4. X-ray Diffraction (XRD)

X-ray studies of the films were performed at room temperature, using Cu Kα radiation (λ = 1.54 Å) at 40 kV and 30 mA (DRONEK 4-AXES Huber Diffractionstechnik GmbH & Co. KG, Germany). The films were mounted on a goniometer. The diffraction intensity data was collected in transmission mode. XRD data was collected with an equatorial (2θ) scan from 2θ = 8 to 30°, at a scanning rate of 0.02° min^{-1} and a 2θ step of 0.2°. XRD results indicated complete dissolution of cellulose was achieved by conversion from Cellulose I to II [58,59]. Results and discussion are included in the supplementary information with Figure S5 [7,8,12,17,22,23,41,54,58–63].

2.5. Dynamic Mechanical Thermal Analysis (DMTA)

All the DMTA tests were performed on a TA Instruments DMA850 under DMTA multifrequency strain mode. A temperature ramp test was performed with a temperature range of −110 to 0 °C; a temperature ramp rate of 3 °C min^{-1}; the frequency was 1 Hz; and the dynamic strain kept between 0.05–0.1% depending on the optimal signal quality [64]. A preload force of 0.1 N was applied to maintain sample tension throughout oscillation. Data is reported as a function of increasing temperature due to reduced system control in descending ramp tests [64]. After testing, peaks were analysed by least squares fitting to gaussian peaks and removal of background noise.

2.6. Thermogravimetric Analysis (TGA)

All TGA tests were performed on a Shimadzu TGA50. Alumina cells with 20 mg samples were used with a nitrogen purge with a flow rate of 50 ml min^{-1}. The temperature ramp rate was 10 K min^{-1} from 30.0–500.0 °C. Weight percentages of each film component were calculated as a percentage of the total weight tested.

2.7. Contact angle testing

Contact angles were measured by an Attension Theta Optical Tensiometer using the sessile drop method. 5 μl of deionised water was placed on the surface of the film and the mean contact angle determined by fitting the Young–Laplace model to each side-profile image of the deposited droplet using automatic baseline detection. To minimise the impact of air-gaps, a drop of water was suspended from a needle, and then the film surface was carefully brought into contact with this hanging droplet. Values reported in Supplementary Figure 5 (b) represents the mean result derived from a minimum of five tests averaged between 30 and 60 s after droplet deposition, obtained from various locations on the film surface. Results and discussion are included in the supplementary information with Figures S6 and S7 [65–71].

3. Results and discussion

3.1. Molecular relaxation mechanisms - DMTA

Temperature ramp tests were performed to understand the effect of composition on the secondary relaxations often correlated with material toughness via the intensity of corresponding tan(δ) peaks [72]. Pure cellulose DMTA studies exhibit a peak between −50 and −80 °C corresponding to γ or β relaxations that have been attributed to a variety of mechanisms [73]. For example, these relaxations have been attributed to hydroxyl side chains in cellulose but could be connected with a hierarchical facilitation of longer scale cooperative relaxations [73,74]. In SF a similar peak is seen around this temperature which is associated to movements of hydrated peptide side chains [64]. Fig. 3 shows the trend for both tan(δ) and the peak position to decrease with addition of SF.

In Fig. 3 (b), the negative trend shown with increasing SF content can be correlated to a reduction in both the total energy of the relaxations occurring, and energetic cost for the associated secondary relaxation event to occur [72]. Guan et al. denote this relaxation in pure SF fibres as $T_{\beta 1}$, due to the loss event (molecular motion/energy dissipation) of axial group motion with peptide-water interactions (See Fig. 4 (a)) [64]. As this trend appears monotonic this motion does not correlate with the bulk non-monotonic trends seen in mechanical analyses (see Section 3.3). However, the sharp decrease in tan(δ) and the peak position with addition of SF deviates from the Fox equation, Gordon and Taylor equation, or linear rules of mixing as seen in Fig. 3(b) [75,76]. This deviation from typical mixing behaviour indicates the blend is not fully miscible and implies the presence of some phase separation, as supported by evidence in Section 3.2[76].

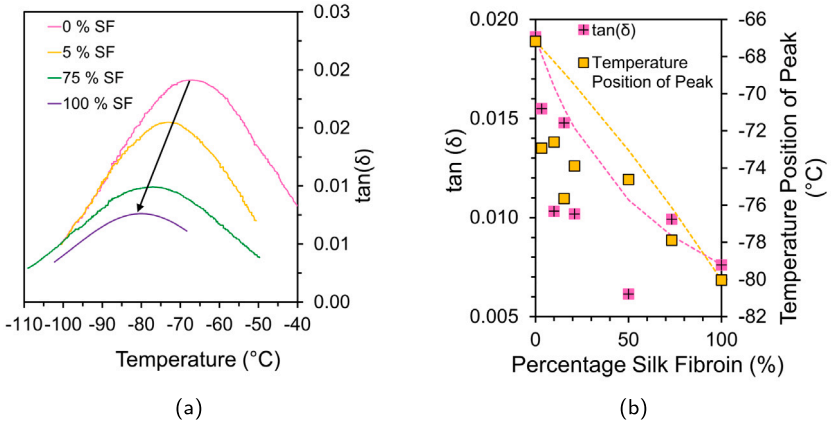

Fig. 3. Graphs showing (a) typical secondary relaxation peaks with background removed at various sample compositions; and (b) trends in tan(δ) and peak position with sample composition. A fitting with the Fox rule has been included to indicate the mixing relationship and deviation from this in the data [75,76].

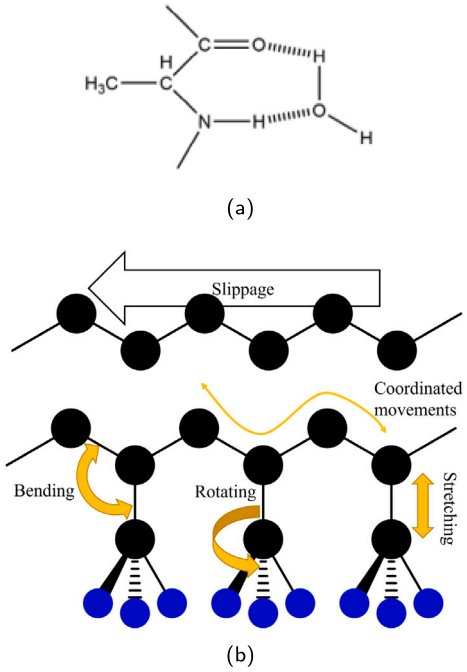

Fig. 4. Diagrams showing (a) SF peptide - water associations for an example alanine amino acid [64]; and (b) the Crankshaft model for motions in a polymer chain [72].

The negative trend shows the increasing ease of side group mobility (reducing temperature of relaxation), and the reducing total side group mobility (reducing amplitude of peak) with additional SF polymer content [72]. This can be visualised with the increasing ease of short lengthscale motions in the Crankshaft model (see Fig. 4(b)). Though plasticisation of these motions can be caused by water or solvents in primary or secondary bound positions [68], it is unlikely water content is the direct cause of this trend due to the similar water contents of different compositions shown in Section 3.2. However, it is possible bonding site accessibility may be impacted by SF addition to cellulose networks. Therefore the bound to free/bulk water ratio change with composition and alter the properties [68]. The adsorption process in cellulose is not always sequential. Increases in system hydration can incur increases in any of the following water states [68]: primary bound water; secondary bound water; free water; bulk water.

3.2. Thermal behaviour - TGA

The results from TGA suggest both partial phase separation and content mixing, due to the presence of peaks attributed to decay of pure and mixed polymer phases (see Fig. 5 (b)). As described by Hadadi et al. and Love et al., thermal decomposition is used to infer the stability of each interface by the temperature required to overcome adhesive forces and incur degradation [12,40]. The mixed polymer phase gives rise to more SF-cellulose interfaces with weaker interactions than those found in pure phases of either polymer [12,40]. This gives rise to three peaks in our signal which can then be used to ascertain the morphology and content of mixed, pure SF, and pure cellulose phases. Our data agrees with similar evidence from Defrates et al. and others who found a distinct peak between 200–300 °C that was attributed to a unique silk-cellulose associated phase [24,54]. This was in addition to peaks attributed to pure cellulose and silk components [24,54]. This implies the presence of phase separated regions of each polymer. Further evidence of this is shown by XRD, in Figure S5, which confirms distinct peaks for the presence of pure silk crystallites and pure cellulose II crystallites in hybrid samples. This provides direct morphological evidence of phase separated regions. Defrates et al. further supported this conclusion with scanning electron microscopy of comparable samples. This showed surface aggregation in hybrid samples at 10%–30% SF content due to partial phase separation [24]. Hadadi et al. also identify partial phase separation between SF and cellulose (with TGA, scanning electron microscopy, and Fourier-transform infrared spectroscopy) encouraged by free energy minimisation during coagulation of the polymer solution [40].

The presence of multiple peaks in the TGA spectra is in contrast to findings by River-Galleti et al. and others [18,41,56]. These papers showed smooth transitions from the lower SF degradation temperature to the pure cellulose degradation temperature with composition change. This implies a homogeneous behaviour and complete mixing between the polymers, but could also be different due to signal overlap between the SF and cellulose peaks. Chain length, or solvent associations can cause variations in the temperature of degradation to occur [77,78]. Zhou et al. saw no peak from mixed content, and only noted two distinct peaks for pure SF and pure cellulose that varied with size [41]. Interestingly, they also noted no non-monotonic peak in mechanical material properties with mixed compositions [41]. This indicates the importance of mixed SF/cellulose associations in hybrid composites, and how they could directly cause the increase in material strength shown in other examples [8].

Our results showed a peak in the total percentage of content in the mixed state between 5%–20% SF. This could correlate with other maxima seen in materials properties testing, indicating the impact of the interaction rich mixing occurring at approximately 10% SF

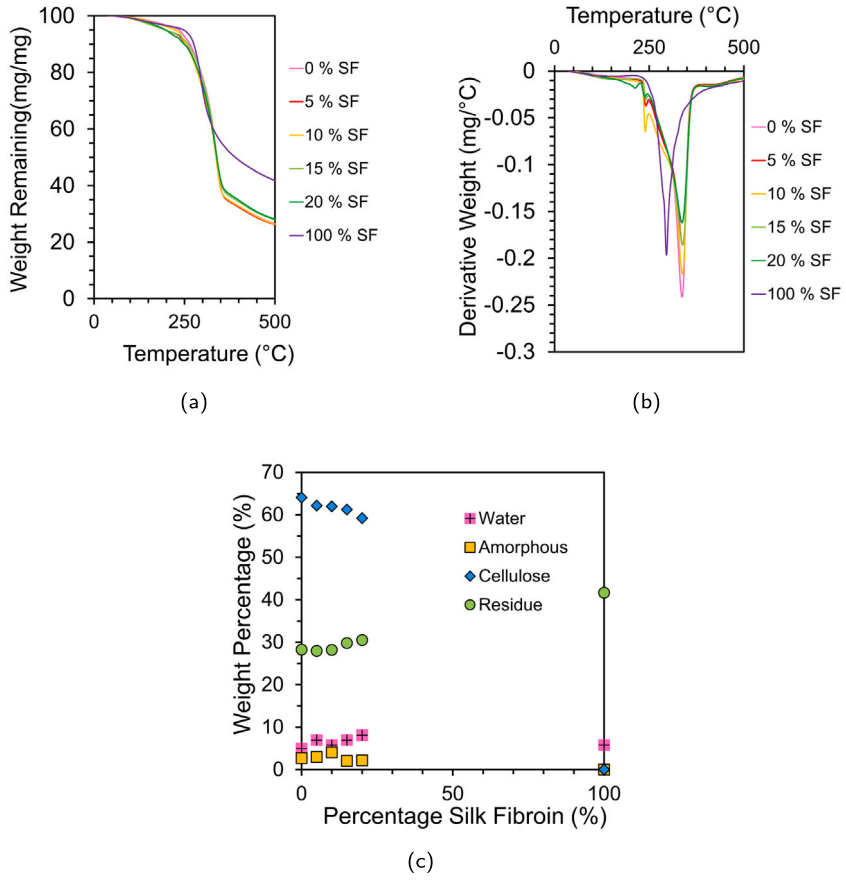

Fig. 5. Graphs showing (a) normalised data of the TGA temperature ramps, and (b) the derivative plot of the resulting TGA analysis, and (c) the % mass of each peak shown as the percentage of the associated decaying component. The analysis method to procure these values is included in the supplementary information with Figure S8.

composition. This could result in more interactions contributing to higher material strengths. A diagram for this hypothesised interspersal and increased interaction density can be seen in Figure S9 [39,79]. Also noted is an increase in the remaining residue after the test with increasing SF content, this implies SF has a lower content of volatile components within the testing range.

3.3. Bulk mechanical analysis - Tensile testing

Mechanical analysis was performed in extension. Different rates of deformation were tested, to understand the impact of time-dependent creep and relaxation on mechanical behaviours. To allow for comparison despite sample dimension variation, typical deflection rates were converted to strain rates in the extensional regime [9,80]. We therefore compared slow (1.5% min^{-1}) and fast (25% min^{-1}) deformation in extensional. These values were selected as extremes of the range of common strain rates seen in literature [80,81]. Values were converted from mm min^{-1} to strain % min^{-1} to make comparisons possible across different sample dimensions. Example stress–strain curves and extracted data averages are shown in Fig. 6.

For all samples a peak in strength and modulus between 5%–15% SF is seen regardless of strain rate. This can be seen in Fig. 6 (c) and (d) and is reflected in equivalent flexural testing tests in Figure S4 (c) and (d). This peak can be understood with generalised modelling of double networks as described by Nakajima [79]. Using fracture energy, (G, J m^{-2}), robustness can be approximated as the resistance to crack propagation causing material failure [79]. The intrinsic fracture energy can be described with Lake-Thomas theory as:

$$G_0 = NU\nu_{area} \quad (3)$$

where N is the number of chemical bonds in a network strand, U is the dissociation energy of the weakest chemical bond (J), and ν_{area} is the area density of effective network strands (m^{-2}) [79]. Hence, the hypothesised increase in both network density and interactions caused by SF interspersal and interactions encourages the increase in material modulus and strength [39]. This is correlated with the presence of a hybrid mixed phase as supported by evidence in Sections 3.1 and 3.2.

Alternatively, Hadadi et al. propose a novel theoretical model that accurately correlates bulk properties and microscopic structures. This indicates an increase in modulus with small additions of SF due to entropic contributions [40]. It proposes that composites form sheets of crystalline monocomposition that reduce the number of interfaces seen [40]. Cohesive energies then depend on the ability to stack and adhere each layer. ‘Gelation’ of these systems does not originate from chemical crosslinking but from competition between interactions. This triggers phase separation to form the biopolymer hydrogel [40]. Entropy in these systems increases rapidly with small additions of a second component, increasing modulus at low weight percentages of SF composition. Compositions closer to 50:50 then show a greater energetic dependence instead [40]. Hence, it is likely the peak in sample modulus is caused by a combination of entropic and enthalpic contributions.

Notably, in the strain at failure comparisons, monotonic decrease is shown with increasing SF content at fast rates of deformation. At slow rates of deformation a non-monotonic trend is seen, as shown in Fig. 6 (e). This shows both conflicting trends shown in literature examples: Zhou et al. showed a monotonic decrease in properties with added SF; and Tian et al. showed a non-monotonic increase in strain at failure [22,41]. This shows the impact of strain rate on the deformation behaviour of samples. With slow deformation sample relaxation occurs in the

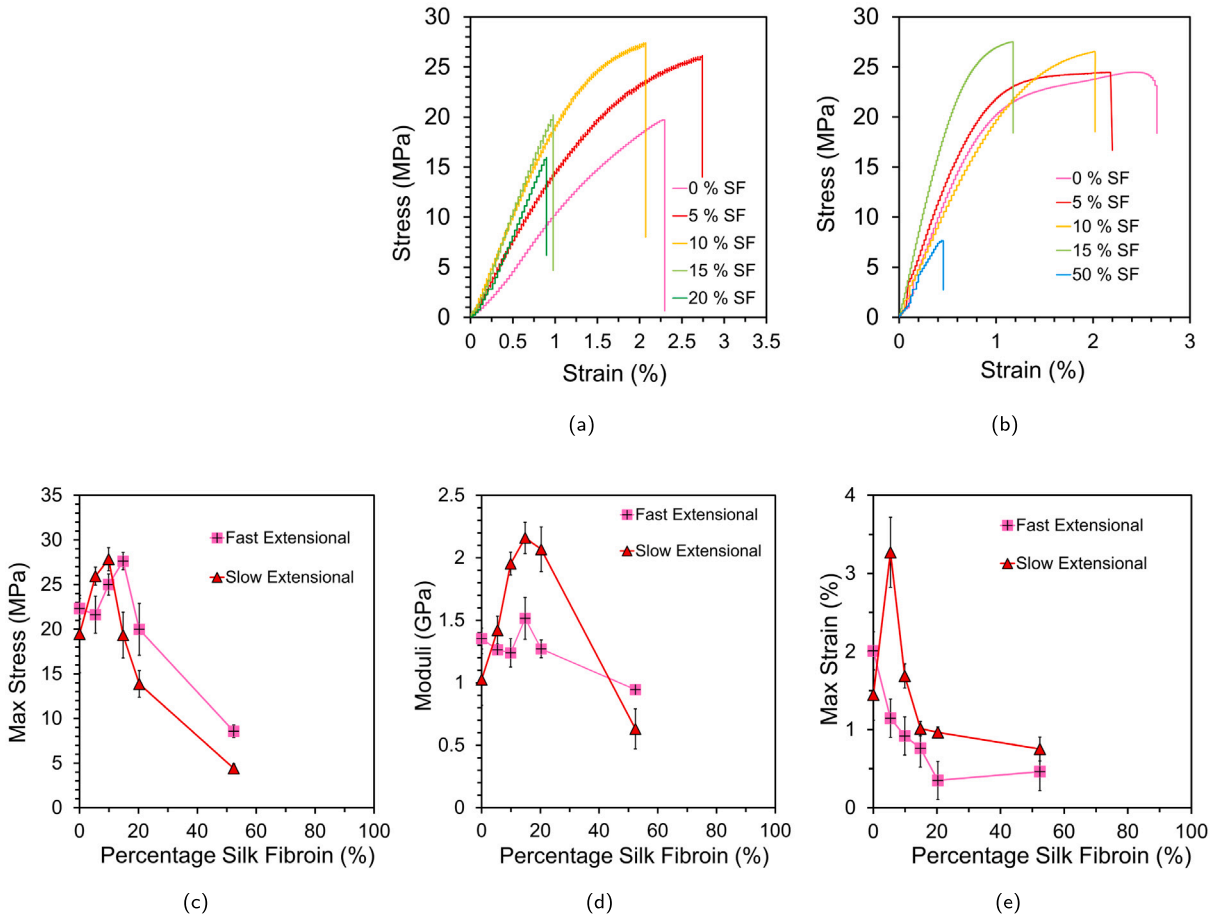

Fig. 6. Graph showing the stress–strain behaviour of films during (a) 'slow' and (b) 'fast' extensional testing with in the extensional regimes. This also shows the extracted average data of the Young's moduli (c), the maximum stress (d), and the strain at failure (e) for 'slow' extensional; and 'fast' extensional tests.

Table 1
Summary of mechanical properties and processing conditions for materials comparable to coagulated hybrid SF and cellulose films in current relevant literature.

Material description	Processing conditions	Mechanical modulus	Reference
Articular cartilage		0.4–1.6 MPa	[81]
Native femoral artery		≈9.0 MPa	[81]
Human medial meniscus		≈1.0 MPa	[81]
20 wt% SF bacterial nanocellulose reinforced composite	SF suspension photocrosslinked to reinforcing cellulose	2.2–14.0 GPa (tensile)	[81]
Fibre reinforced all cellulose composite	Partial dissolution of woven fabric in 1-butyl-3-methylimidazolium acetate and coagulation in water	2.45 GPa (tensile)	[42]
Fibres of silk inspired triblock protein with cellulose binding domains and nanocellulose reinforcement	Extrusion of aqueous solutions and coagulation in ethanol	35 ± 6.3 GPa (tensile)	[23]
10% SF matrix with isotropic cellulose whisker reinforcement	Casting and drying of aqueous mixture	≈11 GPa (tensile)	[17]
Silk fibre		12.7 ± 1.3 GPa	[80]
Coagulated silk film	Silk fibre fully dissolved in EmimAc and coagulated in a methanol atmosphere	1.0 ± 0.4	[80]

hybrid samples between 5%–15% SF allowing greater deformation. This implies the presence of a slow relaxation capable of deforming samples, and imparting rate dependent viscoelastic behaviour. Similar trends in flexural testing data (see Figure S4 (e)) support this conclusion. This viscoelastic behaviour is further investigated in Section 3.4. Variation of this peak between comparable studies and samples shows dependence on mixing, testing conditions, polymer compatibility, and component source as seen in Table 1[8,21,82].

As shown in Table 1, the films produced have lower moduli than aligned filaments and fibres or reinforced undissolved composites. This is due to the isotropy of the polymer network in the film examples. Samples from this study show higher moduli than single component films of other studies. Additionally, the material produced has comparable moduli some with biological systems and hence could act as a promising tissue substitute [21,28,48,49]. Hybrid biomaterials offer a low rejection rate when applied as a biomimetic scaffold for cell or tissue growth and proliferation [10,21,29]. The findings here could be used to develop work by Lee et al. who showed the effective application of SF and bacterial cellulose composites as bioresorbable fixation plates in zygomatic arches of rats [21]. For example, the more effective

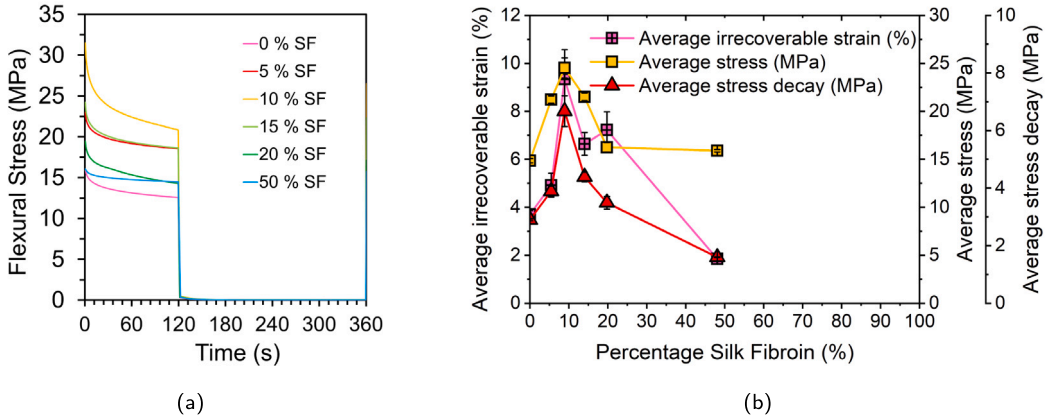

Fig. 7. Graphs showing (a) representative stress relaxation at 1% flexural strain and (b) trends in average irrecoverable strain, average maximum stress, and the average stress decay. The analysis method to procure these values is included in the supplementary information with Figure S10.

solvent system and blending presented in this study could be utilised to better control blend properties of the resulting material. This could be confirmed by biological analysis of cytocompatibility, biodegradation, or sterilisation behaviours in future studies.

3.4. Static mechanical testing

Static testing was performed at both a set strain and stress value. This gave stress relaxation and creep test results, both of which were measured in flexural modes.

3.4.1. Stress relaxation testing

Stress relaxation tests confirmed the increased moduli of hybrid samples, as shown by an increase in the stress applied to achieve the given strain. Interestingly, a larger amount of irrecoverable strain was also seen with these samples after testing. This, as seen in Fig. 7, shows the presence of viscous relaxation behaviour in hybrid samples. This occurs due to the pronounced secondary creep causing stress relaxation over long periods of time for these samples [83]. Diagrams of the analysis performed can be seen in Figure S10.

The presence of a slow relaxation mechanism with small addition of SF could point at a molecular slipping mechanism occurring at these hybrid compositions. The presence of hybrid phases, as confirmed in Section 3.2, with weaker interactions could act as regions of 'sacrificial bonds' as described in double network theory [79]. This could give rise to localised failure, allowing slippage and molecular rearrangement in hybrid samples. This mimics the slippage mechanism also proposed by Mohammadi et al. for cellulose composites with higher lengthscale reinforcement [23]. A visualisation of this mechanism can be seen in Fig. 8.

This also mirrors behaviours shown in more complex biological gels. In studies on extracellular matrices and cytoskeletons, as strain is increased gels stiffen and exhibit faster stress relaxation [48–50]. This dissipates internal stress and elastic energy. This effect is not universal amongst biopolymer networks, but is proposed to occur due to weaker transient bonds, like the hydrogen bonding interactions seen in SF and cellulose hybrids [48–50]. This non-linear response to strain rates also highlights the presence of multiple relaxation times, as indicated by fittings of stretched exponentials with β values between 0.06–0.31 in Table 2. This is used here as an indicative measure of stress relaxation, showing the quickest macroscopic relaxation time at 10% SF content [84]. Further understanding of microscopic relaxation processes could be achieved in follow-on studies with X-ray photon correlation spectroscopy [84]. The non-monotonic increase in stress relaxation differs from the monotonic change in side group mobility shown by DMTA. This indicates the sliding mechanism proposed is mediated by higher order cooperative motion allowed by sacrificial bonds at interfaces.

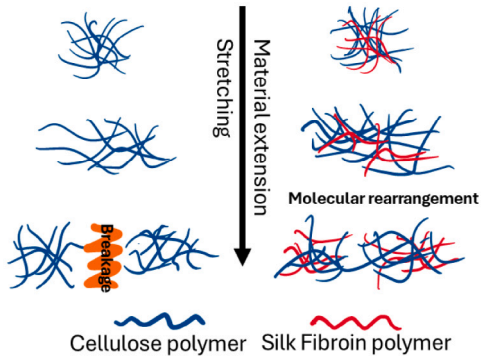

Fig. 8. Diagram indicating the slippage mechanism for molecular rearrangement in hybrid bioplastics, in comparison to pure cellulose failure and breakage.

Table 2
Stretched exponential fitting values showing the stretched exponent, β, and macroscopic relaxation time, τ_M, for samples of different SF compositions during the stress relaxation testing.

SF/%	Stretching exponent	Relaxation time/s
0	0.06	620
5	0.13	650
10	0.15	310
15	0.06	880
20	0.28	710
50	0.15	1250

3.4.2. Creep testing

To confirm theories about the behaviours shown in Sections 3.4.1 and 3.3 we analysed the behaviour of samples under constant stress. This also confirmed the pronounced viscous behaviour shown between 5%–15% SF. This was shown by an increase in total irrecoverable strain and in the total strain over time during creep tests, as shown in Fig. 9.

Under 8 MPa of stress, the purely cellulose film showed a largely elastic behaviour, with little irrecoverable strain seen. With added SF, viscous behaviour was shown by the presence of irrecoverable strain. This could indicate that under this given stress the 'slipping' relaxation mechanism occurred and incurred a secondary, steady state creep to relax the polymer network [83]. This is also reflected in the gradient difference between 15% SF samples and 0% SF samples after 60 s of deformation. This strain behaviour indicates prolonged creep in these samples. This could indicate that the reduced strength of mixed biopolymer interactions allows for these 'sacrificial bonds' to fail under applied stress [8,23]. Higher protein contents caused brittleness as they

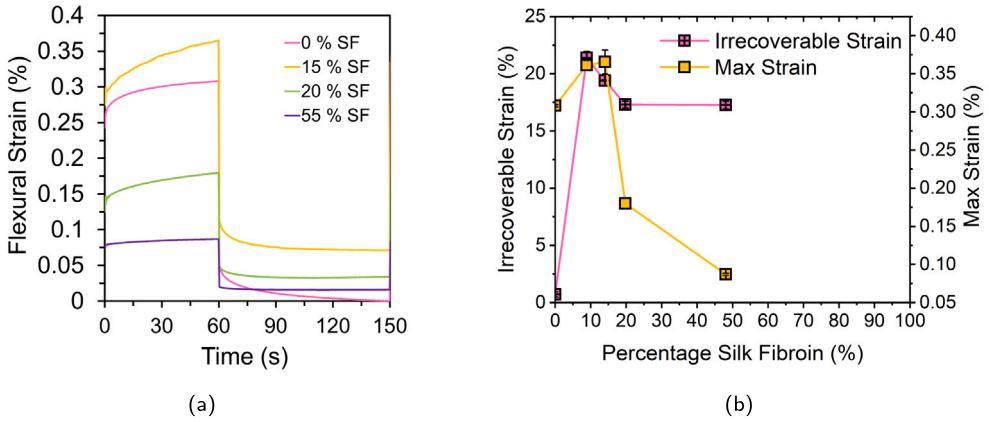

Fig. 9. Graphs showing (a) representative creep test strains for 8 MPa stress application and release (b) trends in average irrecoverable strain and the maximum strain achieved on average. The analysis method to procure these values is included in the supplementary information with Figure S11.

no longer allow for dissipation of energy by reformation of hydrogen bonds [23]. Hence an optimum SF content gives a cohesive matrix. This value was about 30% SF content within the matrix for Mohammadi et al. but is between 5%–15% SF in our study [23]. This may be as a result of various factors including: solvent choice, polymer source, purity, alignment, and polymer chain length [6,8,21,23,32].

4. Conclusions

In this study, we confirm an optimum in material strength and stiffness (28 MPa and 2.2 GPa) with tensile testing at approximately 5%–15% SF compositions. We also demonstrate a dependence of properties on strain rate and confirm, with stress relaxation and creep testing, viscoelastic behaviours characteristic of slow creep and stress relaxation. This material behaviour matches trends shown in complex cytoskeletal examples also possessing transient bonds [48–50]. Both of these behaviours are attributed to the presence of mixed amorphous phase of SF and cellulose indicated by TGA, XRD, and DMTA. This interspersed double network increases interaction density and interfaces, increasing material strength from added enthalpic and entropic contributions. In addition, the failure of 'sacrificial' transient hydrogen bonds under stress within this double network allows network relaxation [23]. This causes a large-scale relaxation which may contribute to conflicting trends previously unexplained in literature.

Further studies should be performed to statistically analyse and model the relaxation behaviour outlined in this work, to provide insight into the molecular relaxation mechanisms involved. Materials could also be explored with Fourier-transform infrared spectroscopy, Raman spectroscopy, and differential scanning calorimetry. Alongside direct morphological characterisation with scanning electron microscopy, these techniques could be used to further confirm observations from this work. Increasing the lengthscale of reinforcement and comparing material properties could offer insight into further optimisations possible with this system; as aligned reinforcements showed higher material toughness than isotropic dispersed fibre reinforcements [7,85]. The fully dissolved film from this study could act as an effective matrix for a self-reinforced composite with high performance to better implement these materials as biomimetic tissue replacements.

Abbreviations

The following abbreviations are used in this manuscript:

SF	Silk Fibroin
XRD	X-ray Diffraction
DMTA	Dynamic Mechanical Thermal Analysis
TGA	Thermogravimetric Analysis
FTIR	Fourier-Transform Infrared Spectroscopy

CRediT authorship contribution statement

James A. King: Writing – review & editing, Writing – original draft, Validation, Methodology, Investigation, Formal analysis, Data curation, Conceptualization. **Peter J. Hine:** Writing – review & editing, Validation, Supervision, Resources. **Daniel L. Baker:** Writing – review & editing, Validation, Supervision, Resources. **Matthew Creswick:** Writing – review & editing, Validation, Investigation, Data curation. **Michael E. Ries:** Writing – review & editing, Validation, Supervision, Investigation, Data curation.

Funding

James King was supported by the EPSRC CDT in Soft Matter for Formulation and Industrial Innovation, "SOFI^2", (EP/S023631/1).

Declaration of competing interest

The authors declare the following financial interests/personal relationships which may be considered as potential competing interests: James Andrew King reports financial support was provided by the Engineering and Physical Sciences Research Council. If there are other authors, they declare that they have no known competing financial interests or personal relationships that could have appeared to influence the work reported in this paper.

Acknowledgements

With special thanks to support and guidance from my supervisory team of Mike, Peter, and Dan. Thank you for supporting work from Adrian Cunliffe at SCAPE, and to Matthew Creswick for his contact angles work and interpretation. Lastly, huge appreciation to my sister, Helen, without whom I wouldn't be a scientist and who helped write all code used in this work. Thank you for inspiring me.

Appendix A. Supplementary data

All data needed to evaluate the conclusions in the paper are present in the paper and/or the Supplementary Materials. In addition, the data associated with this paper are openly available from the University of Leeds Data Repository at https://doi.org/10.5518/1677.

Supplementary material related to this article can be found online at https://doi.org/10.1016/j.ijbiomac.2025.145931.

References

[1] H. Baniasadi, Z. Fathi, C.D. Cruz, R. Abidnejad, P. Tammela, J. Niskanen, E. Lizundia, Structure-property correlations and environmental impact assessment of sustainable antibacterial food packaging films reinforced with fungal chitin nanofibrils, Food Hydrocolloids 162 (October 2024) (2025) http://dx.doi.org/10.1016/j.foodhyd.2024.110987.

[2] R. Abidnejad, H. Baniasadi, M. Fazeli, S. Lipponen, E. Kontturi, O.J. Rojas, B.D. Mattos, High-fiber content composites produced from mixed textile waste: Balancing cotton and polyester fibers for improved composite performance, Int. J. Biiol. Macromol. 292 (October 2024) (2025) 139227, http://dx.doi.org/10.1016/j.ijbiomac.2024.139227.

[3] J. Eom, S. Park, H.J. Jin, H.W. Kwak, Multiscale hybridization of natural silk–nanocellulose fibrous composites with exceptional mechanical properties, Front. Mater. 7 (May) (2020) 1–12, http://dx.doi.org/10.3389/fmats.2020.00098.

[4] H. Baniasadi, Z. Fathi, E. Lizundia, C.D. Cruz, R. Abidnejad, M. Fazeli, P. Tammela, E. Kontturi, J. Lipponen, J. Niskanen, Development and characterization of pomegranate peel extract-infused carboxymethyl cellulose composite films for functional, sustainable food packaging, Food Hydrocolloids 158 (August 2024) (2025) http://dx.doi.org/10.1016/j.foodhyd.2024.110525.

[5] B. Baghaei, M. Skrifvars, All-cellulose composites: A review of recent studies on structure, properties and applications, Molecules 25 (12) (2020) http://dx.doi.org/10.3390/molecules25122836.

[6] L. Ciobanu, Development of 3D knitted fabrics for advanced composite materials, in: Advances in Composite Materials - Ecodesign and Analysis, InTech, 2011, http://dx.doi.org/10.5772/14876, URL https://api.semanticscholar.org/CorpusID:136557679.

[7] C. Cianci, D. Chelazzi, G. Poggi, F. Modi, R. Giorgi, M. Laurati, Hybrid fibroin-nanocellulose composites for the consolidation of aged and historical silk, Colloids Surfaces A: Physicochem. Eng. Asp. 634 (November 2021) (2022) 127944, http://dx.doi.org/10.1016/j.colsurfa.2021.127944.

[8] M. Kostag, K. Jedvert, O.A. El Seoud, Engineering of sustainable biomaterial composites from cellulose and silk fibroin: Fundamentals and applications, Int. J. Biiol. Macromol. 167 (2021) 687–718, http://dx.doi.org/10.1016/j.ijbiomac.2020.11.151.

[9] A. Victoria, M. Edward Ries, P. John Hine, Use of interleaved films to enhance the properties of all-cellulose composites, Compos. Part A: Appl. Sci. Manuf. 160 (March) (2022) 107062, http://dx.doi.org/10.1016/j.compositesa.2022.107062.

[10] J.A. King, X. Zhang, M.E. Ries, The formation of all-silk composites and time–temperature superposition, Materials 16 (10) (2023) http://dx.doi.org/10.3390/ma16103804.

[11] Mayank, A. Bardenhagen, V. Sethi, H. Gudwani, Spider-silk composite material for aerospace application, Acta Astronaut. 193 (February 2021) (2022) 704–709, http://dx.doi.org/10.1016/j.actaastro.2021.08.013.

[12] S.A. Love, X. Hu, D. Salas-de la Cruz, Controlling the structure and properties of semi-crystalline cellulose/silk-fibroin biocomposites by ionic liquid type and hydrogen peroxide concentration, Carbohydr. Polym. Technol. Appl. 3 (February) (2022) 100193, http://dx.doi.org/10.1016/j.carpta.2022.100193.

[13] M. Nasir, R. Hashim, O. Sulaiman, M. Asim, Nanocellulose: Preparation methods and applications, Cellulose- Reinf. Nanofibre Compos.: Prod. Prop. Appl. 11 (2017) 261–276, http://dx.doi.org/10.1016/B978-0-08-100957-4.00011-5.

[14] A.D. French, Glucose, not cellobiose, is the repeating unit of cellulose and why that is important, Cellulose 24 (11) (2017) 4605–4609, http://dx.doi.org/10.1007/s10570-017-1450-3.

[15] M.E. Ries, P.J. Hine, L. Mancell, Circular is the new black, Mater. World (2020) 27–29.

[16] O.A. El Seoud, K. Jedvert, M. Kostag, S. Possidonio, Cellulose, chitin and silk: the cornerstones of green composites, Emergent Mater. 5 (2021) 785–810, http://dx.doi.org/10.1007/s42247-021-00308-0.

[17] Y. Noishiki, Y. Nishiyama, M. Wada, S. Kuga, J. Magoshi, Mechanical properties of silk fibroin-microcrystalline cellulose composite films, J. Appl. Polym. Sci. 86 (13) (2002) 3425–3429, http://dx.doi.org/10.1002/app.11370.

[18] B. Blessing, C. Trout, A. Morales, K. Rybacki, S.A. Love, G. Lamoureux, S.M. O'malley, X. Hu, D. Salas-De la Cruz, The impact of composition and morphology on ionic conductivity of silk/cellulose bio-composites fabricated from ionic liquid and varying percentages of coagulation agents, Int. J. Mol. Sci. 21 (13) (2020) 1–23, http://dx.doi.org/10.3390/ijms21134695.

[19] K. Wang, Q. Ma, Y.M. Zhang, G.T. Han, C.X. Qu, S.D. Wang, Preparation of bacterial cellulose/silk fibroin double-network hydrogel with high mechanical strength and biocompatibility for artificial cartilage, Cellulose 27 (4) (2020) 1845–1852, http://dx.doi.org/10.1007/s10570-019-02869-0.

[20] S. Guzman-Puyol, J.A. Heredia-Guerrero, L. Ceseracciu, H. Hajiali, C. Canale, A. Scarpellini, R. Cingolani, I.S. Bayer, A. Athanassiou, E. Mele, Low-cost and effective fabrication of biocompatible nanofibers from silk and cellulose-rich materials, ACS Biomater. Sci. Eng. 2 (4) (2016) 526–534, http://dx.doi.org/10.1021/acsbiomaterials.5b00500.

[21] J.M. Lee, J.H. Kim, O.J. Lee, C.H. Park, The fixation effect of a silk fibroin-bacterial cellulose composite plate in segmental defects of the zygomatic arch: An experimental study, JAMA Otolaryngol. - Head Neck Surg. 139 (6) (2013) 629–635, http://dx.doi.org/10.1001/jamaoto.2013.3044.

[22] D. Tian, T. Li, R. Zhang, Q. Wu, T. Chen, P. Sun, A. Ramamoorthy, Conformations and intermolecular interactions in cellulose/silk fibroin blend films: A solid-state NMR perspective, J. Phys. Chem. B 121 (25) (2017) 6108–6116, http://dx.doi.org/10.1021/acs.jpcb.7b02838.

[23] P. Mohammadi, A.S. Aranko, C.P. Landowski, O. Ikkala, K. Jaudzems, W. Wagermaier, M.B. Linder, Biomimetic composites with enhanced toughening using silk-inspired triblock proteins and aligned nanocellulose reinforcements, Sci. Adv. 5 (9) (2019) http://dx.doi.org/10.1126/sciadv.aaw2541.

[24] K. DeFrates, T. Markiewicz, K. Callaway, Y. Xue, J. Stanton, D. Salas-de la Cruz, X. Hu, Structure–property relationships of thai silk–microcrystalline cellulose biocomposite materials fabricated from ionic liquid, Int. J. Biiol. Macromol. 104 (2017) 919–928, http://dx.doi.org/10.1016/j.ijbiomac.2017.06.103.

[25] R. Pramanik, A. Arockiarajan, Mechanical and morphological characterization of a novel silk/cellulose-based soft composite, Mater. Lett. 314 (January) (2022) 131871, http://dx.doi.org/10.1016/j.matlet.2022.131871.

[26] R. Eivazzadeh-Keihan, F. Ahmadpour, H.A.M. Aliabadi, F. Radinekiyan, A. Maleki, H. Madanchi, M. Mahdavi, A.E. Shalan, S. Lanceros-Méndez, Pectin-cellulose hydrogel, silk fibroin and magnesium hydroxide nanoparticles hybrid nanocomposites for biomedical applications, Int. J. Biiol. Macromol. 192 (September) (2021) 7–15, http://dx.doi.org/10.1016/j.ijbiomac.2021.09.099.

[27] V. Narayanan, S. Sumathi, Preparation, characterization and in vitro biological study of silk fiber/methylcellulose composite for bone tissue engineering applications, Polym. Bull. 76 (6) (2019) 2777–2800, http://dx.doi.org/10.1007/s00289-018-2518-4.

[28] C. Holland, K. Numata, J. Rnjak-Kovacina, F.P. Seib, The biomedical use of silk: Past, present, future, Adv. Heal. Mater. 8 (1) (2019) http://dx.doi.org/10.1002/adhm.201800465.

[29] S. Tandon, B. Kandasubramanian, S.M. Ibrahim, Silk-based composite scaffolds for tissue engineering applications, Ind. Eng. Chem. Res. 59 (40) (2020) 17593–17611, http://dx.doi.org/10.1021/acs.iecr.0c02195.

[30] Z.J. Chen, Y. Zhang, L. Zheng, H. Zhang, H.H. Shi, X.C. Zhang, B. Liu, Mineralized self-assembled silk fibroin/cellulose interpenetrating network aerogel for bone tissue engineering, Mater. Sci. Eng. C 134 (November 2021) (2021) 112549, http://dx.doi.org/10.1016/j.msec.2021.112549.

[31] P. Ang-atikarnkul, A. Watthanaphanit, R. Rujiravanit, Fabrication of cellulose nanofiber/chitin whisker/silk sericin bionanocomposite sponges and characterizations of their physical and biological properties, Compos. Sci. Technol. 96 (2014) 88–96, http://dx.doi.org/10.1016/j.compscitech.2014.03.006.

[32] B.N. Singh, K. Pramanik, Generation of bioactive nano-composite scaffold of nanobioglass/silk fibroin/carboxymethyl cellulose for bone tissue engineering, J. Biomater. Sci. Polym. Ed. 29 (16) (2018) 2011–2034, http://dx.doi.org/10.1080/09205063.2018.1523525.

[33] J. Chen, A. Zhuang, H. Shao, X. Hu, Y. Zhang, Robust silk fibroin/bacterial cellulose nanoribbon composite scaffolds with radial lamellae and intercalation structure for bone regeneration, J. Mater. Chem. B 5 (20) (2017) 3640–3650, http://dx.doi.org/10.1039/c7tb00485k.

[34] X. Cao, J. Li, W. Zhai, B. Zhou, H. Lin, Y. Wang, Inhibiting friction-induced exogenous adhesion via robust lubricative core-shell nanofibers for high-quality tendon repair, Biomacromolecules (2025) http://dx.doi.org/10.1021/acs.biomac.4c01729.

[35] S. Cheng, J. Yang, J. Song, X. Cao, B. Zhou, L. Yang, C. Li, Y. Wang, A motion-responsive injectable lubricative hydrogel for efficient Achilles tendon adhesion prevention, in: Materials Today Bio, vol. 30, 2025, http://dx.doi.org/10.1016/j.mtbio.2025.101458.

[36] Y. Feng, X. Li, M. Li, D. Ye, Q. Zhang, R. You, W. Xu, Facile preparation of biocompatible silk fibroin/cellulose nanocomposite films with high mechanical performance, ACS Sustain. Chem. Eng. 5 (7) (2017) 6227–6236, http://dx.doi.org/10.1021/acssuschemeng.7b01161.

[37] G. Carrasco-Torres, M.A. Valdés-Madrigal, V.R. Vásquez-Garzón, R. Baltiérrez-Hoyos, E.D. De la Cruz-Burelo, R. Román-Doval, A.A. Valencia-Lazcano, Effect of silk fibroin on cell viability in electrospun scaffolds of polyethylene oxide, Polymers 11 (3) (2019) http://dx.doi.org/10.3390/polym11030451.

[38] K. Ganguly, H. Jin, S.D. Dutta, D.K. Patel, T.V. Patil, K.T. Lim, Magnetic field-assisted aligned patterning in an alginate-silk fibroin/nanocellulose composite for guided wound healing, Carbohydr. Polymers 287 (March) (2022) 119321, http://dx.doi.org/10.1016/j.carbpol.2022.119321.

[39] S. Shang, L. Zhu, J. Fan, Physical properties of silk fibroin/cellulose blend films regenerated from the hydrophilic ionic liquid, Carbohydr. Polymers 86 (2) (2011) 462–468, http://dx.doi.org/10.1016/j.carbpol.2011.04.064.

[40] A. Hadadi, J.W. Whittaker, D.E. Verrill, X. Hu, L. Larini, D. Salas-De La Cruz, A hierarchical model to understand the processing of polysaccharides/protein-based films in ionic liquids, Biomacromolecules 19 (10) (2018) 3970–3982, http://dx.doi.org/10.1021/acs.biomac.8b00903.

[41] L. Zhou, Q. Wang, J. Wen, X. Chen, Z. Shao, Preparation and characterization of transparent silk fibroin/cellulose blend films, Polymer 54 (18) (2013) 5035–5042, http://dx.doi.org/10.1016/j.polymer.2013.07.002.

[42] T. Huber, S. Pang, M.P. Staiger, All-cellulose composite laminates, Compos. Part A: Appl. Sci. Manuf. 43 (10) (2012) 1738–1745, http://dx.doi.org/10.1016/j.compositesa.2012.04.017.

[43] B. Azimi, H. Maleki, V. Gigante, R. Bagherzadeh, A. Mezzetta, M. Milazzo, L. Guazzelli, P. Cinelli, A. Lazzeri, S. Danti, Cellulose-based fiber spinning processes using ionic liquids, in: Cellulose, vol. 29, Springer Netherlands, 2022, pp. 3079–3129, http://dx.doi.org/10.1007/s10570-022-04473-1.
[44] Y. Xi, L. Zhang, Y. Tian, J. Song, J. Ma, Z. Wang, Rapid dissolution of cellulose in an AlCl3/ZnCl2aqueous system at room temperature and its versatile adaptability in functional materials, Green Chem. 24 (2) (2022) 885–897, http://dx.doi.org/10.1039/d1gc03918k.
[45] X. Li, H. Li, T. You, X. Chen, S. Ramaswamy, Y.Y. Wu, F. Xu, Enhanced dissolution of cotton cellulose in 1-allyl-3-methylimidazolium chloride by the addition of metal chlorides, ACS Sustain. Chem. Eng. 7 (23) (2019) 19176–19184, http://dx.doi.org/10.1021/acssuschemeng.9b05159.
[46] N. Soykeabkaew, N. Arimoto, T. Nishino, T. Peijs, All-cellulose composites by surface selective dissolution of aligned ligno-cellulosic fibres, Compos. Sci. Technol. 68 (10–11) (2008) 2201–2207, http://dx.doi.org/10.1016/j.compscitech.2008.03.023.
[47] A. Victoria, P.J. Hine, K. Ward, M.E. Ries, Design of experiments in the optimization of all-cellulose composites, Cellulose 30 (17) (2023) 11013–11039, http://dx.doi.org/10.1007/s10570-023-05535-8.
[48] S. Chen, C.P. Broedersz, T. Markovich, F.C. MacKintosh, Nonlinear stress relaxation of transiently crosslinked biopolymer networks, Phys. Rev. E 104 (3) (2021) 1–14, http://dx.doi.org/10.1103/PhysRevE.104.034418, arXiv:2104.11868.
[49] S. Nam, K.H. Hu, M.J. Butte, O. Chaudhuri, Strain-enhanced stress relaxation impacts nonlinear elasticity in collagen gels, Proc. Natl. Acad. Sci. USA 113 (20) (2016) 5492–5497, http://dx.doi.org/10.1073/pnas.1523906113.
[50] Y. Mulla, F.C. Mackintosh, G.H. Koenderink, Origin of slow stress relaxation in the cytoskeleton, Phys. Rev. Lett. 122 (21) (2019) 218102, http://dx.doi.org/10.1103/PhysRevLett.122.218102, arXiv:1810.08165.
[51] Z.J. Chen, H.H. Shi, L. Zheng, H. Zhang, Y.Y. Cha, H.X. Ruan, Y. Zhang, X.C. Zhang, A new cancellous bone material of silk fibroin/cellulose dual network composite aerogel reinforced by nano-hydroxyapatite filler, Int. J. Biiol. Macromol. 182 (2021) 286–297, http://dx.doi.org/10.1016/j.ijbiomac.2021.03.204.
[52] Y. Tomimatsu, H. Suetsugu, Y. Yoshimura, A. Shimizu, The solubility of cellulose in binary mixtures of ionic liquids and dimethyl sulfoxide: Influence of the anion, J. Mol. Liq. 279 (2019) 120–126, http://dx.doi.org/10.1016/j.molliq.2019.01.093.
[53] J.A. King, P.J. Hine, D.L. Baker, M.E. Ries, Understanding the dissolution of cellulose and silk fibroin in 1-ethyl-3-methylimidazolium acetate and dimethyl sulphoxide for application in hybrid films, Materials 17 (21) (2024) 5262, http://dx.doi.org/10.3390/ma17215262, URL https://www.mdpi.com/1996-1944/17/21/5262.
[54] J. Stanton, Y. Xue, J.C. Waters, A. Lewis, D. Cowan, X. Hu, D.S. de la Cruz, Structure–property relationships of blended polysaccharide and protein biomaterials in ionic liquid, Cellulose 24 (4) (2017) 1775–1789, http://dx.doi.org/10.1007/s10570-017-1208-y.
[55] K. Wang, R.S. Hazra, Q. Ma, L. Jiang, Z. Liu, Y. Zhang, S. Wang, G. Han, Multifunctional silk fibroin/PVA bio-nanocomposite films containing TEMPO-oxidized bacterial cellulose nanofibers and silver nanoparticles, Cellulose 29 (3) (2022) 1647–1666, http://dx.doi.org/10.1007/s10570-021-04369-6.
[56] A. Rivera-Galletti, C.R. Gough, F. Kaleem, M. Burch, C. Ratcliffe, P. Lu, D. Salas-De la Cruz, X. Hu, Silk-cellulose acetate biocomposite materials regenerated from ionic liquid, Polymers 13 (17) (2021) http://dx.doi.org/10.3390/polym13172911.
[57] S. Timoshenko, Strength of Materials, third ed., Van Nostrand, Princeton, 1956.
[58] C. Verma, A. Mishra, S. Chauhan, P. Verma, V. Srivastava, M.A. Quraishi, E.E. Ebenso, Dissolution of cellulose in ionic liquids and their mixed cosolvents: A review, Sustain. Chem. Pharm. 13 (July) (2019) 100162, http://dx.doi.org/10.1016/j.scp.2019.100162.
[59] K.M. Gupta, J. Jiang, Cellulose dissolution and regeneration in ionic liquids: A computational perspective, Chem. Eng. Sci. 121 (2015) 180–189, http://dx.doi.org/10.1016/j.ces.2014.07.025.
[60] S.A. Love, E. Popov, K. Rybacki, X. Hu, D. Salas-de la Cruz, Facile treatment to fine-tune cellulose crystals in cellulose-silk biocomposites through hydrogen peroxide, Int. J. Biiol. Macromol. 147 (2020) 569–575, http://dx.doi.org/10.1016/j.ijbiomac.2020.01.100.
[61] A.D. French, Increment in evolution of cellulose crystallinity analysis, in: Cellulose, vol. 27, (10) 2020, pp. 5445–5448, http://dx.doi.org/10.1007/s10570-020-03172-z.
[62] S. Park, J.O. Baker, M.E. Himmel, P.A. Parilla, D.K. Johnson, Cellulose crystallinity index: measurement techniques and their impact on interpreting cellulase performance, Biotechnol. Biofuels 3 (2010) http://dx.doi.org/10.1186/1754-6834-3-10.
[63] B.D. Cullity, S.R. Stock, Elements of X-ray Diffraction, third ed., Prentice Hall, 2001.
[64] J. Guan, D. Porter, F. Vollrath, Thermally induced changes in dynamic mechanical properties of native silks, Biomacromolecules 14 (3) (2013) 930–937, http://dx.doi.org/10.1021/bm400012k.
[65] T. Huhtamäki, X. Tian, J.T. Korhonen, R.H. Ras, Surface-wetting characterization using contact-angle measurements, Nat. Protoc. 13 (7) (2018) 1521–1538, http://dx.doi.org/10.1038/s41596-018-0003-z.
[66] X. Liu, Z. Qin, Y. Ma, H. Liu, X. Wang, Cellulose-based films for food packaging applications: Review of preparation, properties, and prospects, J. Renew. Mater. 11 (8) (2023) 3203–3225, http://dx.doi.org/10.32604/jrm.2023.027613.
[67] M.A. Hubbe, D.J. Gardner, W. Shen, Contact angles and wettability of cellulosic surfaces: A review of proposed mechanisms and test strategies, BioResources 10 (4) (2015) 8657–8749, http://dx.doi.org/10.15376/biores.10.4.Hubbe_Gardner_Shen.
[68] M.F. Froix, R. Nelson, Interaction of water with cellulose from nuclear magnetic resonance relaxation times, Macromolecules 8 (6) (1975) 726–730.
[69] S. Wang, T. Huang, C. Lai, T. Xi, S. Liao, F. Nan, Oxidized nano-bacterial cellulose/silk fibroin composite films, Cellul. Chem. Technol. 50 (7–8) (2016) 853–862.
[70] S. Kaewpirom, S. Piboonnithikasem, P. Sroisroemsap, S. Uttoom, S. Boonsang, Tailoring silk fibroin hydrophilicity and physicochemical properties using sugar alcohols for medical device coatings, Sci. Rep. 14 (1) (2024) 1–14, http://dx.doi.org/10.1038/s41598-024-64450-5.
[71] S. Rbihi, A. Aboulouard, L. Laallam, A. Jouaiti, Contact angle measurements of cellulose based thin film composites: wettability, surface free energy and surface hardness, in: Surfaces and Interfaces, vol. 21, 2020, http://dx.doi.org/10.1016/j.surfin.2020.100708.
[72] K. Menard, Dynamic Mechanical Analysis: A Practical Introduction, second ed., CRC Press, Boca Raton, 2008.
[73] S.A. Bradley, S.H. Carr, Mechanical loss processes in polysaccharides, J. Polym. Sci. Polym. Phys. Ed. 14 (1) (1976) 111–124, http://dx.doi.org/10.1002/pol.1976.180140109.
[74] D.L. Baker, M. Reynolds, R. Masurel, P.D. Olmsted, J. Mattsson, Cooperative intramolecular dynamics control the chain-length-dependent glass transition in polymers, Phys. Rev. X 12 (2) (2022) http://dx.doi.org/10.1103/PhysRevX.12.021047, arXiv:1911.13278.
[75] P.C. Hiemenz, T. Lodge, Polymer Chemistry, second ed., 2007, p. 587, URL https://www.eng.uc.edu/{~}beaucag/Classes/Properties/Books/PaulC.Hiemenz,TimothyP.Lodge-PolymerChemistry-CRCPress(2007).pdf.
[76] W. Brostow, R. Chiu, I.M. Kalogeras, A. Vassilikou-Dova, Prediction of glass transition temperatures: Binary blends and copolymers, Mater. Lett. 62 (17–18) (2008) 3152–3155, http://dx.doi.org/10.1016/j.matlet.2008.02.008.
[77] E. Fischer Kerche, R. Neves, H. Ornaghi Jr., A.J. Zattera, H. Stephan Schrekker, The influence of ionic liquid concentration on microcrystalline cellulose surface modification, SSRN Electron. J. 3 (April) (2022) 0–9, http://dx.doi.org/10.2139/ssrn.4063476.
[78] A. Abdulkhani, M. Daliri Sousefi, A. Ashori, G. Ebrahimi, Preparation and characterization of sodium carboxymethyl cellulose/silk fibroin/graphene oxide nanocomposite films, Polym. Test. 52 (2016) 218–224, http://dx.doi.org/10.1016/j.polymertesting.2016.03.020.
[79] T. Nakajima, Generalization of the sacrificial bond principle for gel and elastomer toughening, Polym. J. 49 (6) (2017) 477–485, http://dx.doi.org/10.1038/pj.2017.12.
[80] X. Zhang, M.E. Ries, P.J. Hine, Time-temperature superposition of the dissolution of silk fibers in the ionic liquid 1-ethyl-3-methylimidazolium acetate, Biomacromolecules 22 (3) (2021) 1091–1101, http://dx.doi.org/10.1021/acs.biomac.0c01467.
[81] P. Dorishetty, R. Balu, S.S. Athukoralalage, T.L. Greaves, J. Mata, L. De Campo, N. Saha, A.C. Zannettino, N.K. Dutta, N.R. Choudhury, Tunable biomimetic hydrogels from silk fibroin and nanocellulose, ACS Sustain. Chem. Eng. 8 (6) (2020) 2375–2389, http://dx.doi.org/10.1021/acssuschemeng.9b05317.
[82] E. Kontturi, T. Tammelin, M. Österberg, Cellulose—model films and the fundamental approach, Chem. Soc. Rev. 35 (12) (2006) 1287–1304, http://dx.doi.org/10.1039/b601872f.
[83] N.E. Dowling, Mechanical Behaviour of Materials: Engineering Methods for Deformation, Fracture, and Fatigue, fourth ed., Pearson, 2013.
[84] J. Song, Q. Zhang, F. De Quesada, M.H. Rizvi, J.B. Tracy, J. Ilavsky, S. Narayanan, E. Del Gado, R.L. Leheny, N. Holten-Anderse, G.H. McKinley, Microscopic dynamics underlying the stress relaxation of arrested soft materials, Proc. Natl. Acad. Sci. USA 119 (30) (2022) 1–8, http://dx.doi.org/10.1073/pnas.2201566119.
[85] A.V. Nadhan, A.V. Rajulu, R. Li, J. Cai, L. Zhang, Properties of waste silk short fiber/cellulose green composite films, J. Compos. Mater. 46 (1) (2012) 123–127, http://dx.doi.org/10.1177/0021998311410507.